Available online at www.sciencedirect.com

SciVerse ScienceDirect

Ceramics International 38 (2012) 1927–1935

CERAMICS INTERNATIONAL

www.elsevier.com/locate/ceramint

Effects of CdF_2 and WO_3 additions on the microstructural and thermal properties of TeO_2–CdF_2–WO_3 glass system

Demet Tatar [a,*], M. Lütfi Öveçoğlu [a], Gönül Özen [b]

[a] Istanbul Technical University, Faculty of Chemical and Metallurgical Engineering, Metallurgical and Materials Science Engineering Department, Maslak, Istanbul 34469, Turkey

[b] Istanbul Technical University, Faculty of Science and Letters, Physics Engineering Department, Maslak, Istanbul 34649, Turkey

Received 21 July 2011; accepted 10 October 2011
Available online 15 October 2011

Abstract

This paper presents microstructural characterization investigations and the crystallization behavior of some glasses in the ternary TeO_2–CdF_2–WO_3 system. Differential thermal analysis (DTA) showed that the glass forming ability of the ternary TeO_2–CdF_2–WO_3 system which is in between the values of 21 and 34, is lower than most of the studied tellurite glasses. It is possible to obtain amorphous glass structure for the compositions of $0.80TeO_2$–$0.10CdF_2$–$0.10WO_3$ and $0.75TeO_2$–$0.10CdF_2$–$0.15WO_3$. On the other hand, the $0.85TeO_2$–$0.10CdF_2$–$0.05WO_3$ and $0.75TeO_2$–$0.15CdF_2$–$0.10WO_3$ compositions do not form glass with conventional quenching techniques. During crystallization of these glasses, the formation of the alpha, delta and gamma TeO_2, WO_3 and $CdTe_2O_5$ phases were observed with the addition of a new unidentified phase. Three compositions of $0.85TeO_2$–$0.10CdF_2$–$0.05WO_3$, $0.80TeO_2$–$0.10CdF_2$–$0.10WO_3$ and $0.75TeO_2$–$0.10CdF_2$–$0.15WO_3$ demonstrated two exothermic peaks in the DTA curves. SEM/EDS investigations confirmed the existence of the alpha, delta and gamma TeO_2, WO_3 and $CdTe_2O_5$ phases for the annealed glasses. The microstructure of the δ-TeO_2 phase was clearly observed in the as-cast $0.75TeO_2$–$0.10CdF_2$–$0.15WO_3$ composition.

Keywords: C. Thermal properties; D. Glass–ceramic; Tellurite glass; Crystallization; Microstructure; X-ray diffractometry

1. Introduction

Tellurium oxide-based glasses are demanded particularly for optical applications because of their promising electrical and optical properties such as high refractive index, high dielectric constant, and good infrared transmissivity [1–18]. In comparison with the silicate glasses, tellurite glasses have less phonon energy, lower melting temperatures and more transparency in the near infrared region [1,2]. Tellurite glasses are preferred over the phosphate glasses since the latter ones have limited bandwidth for amplifications and have low phonon energy [2]. Since tellurium oxide-based glasses have the highest non-linear optical indices among the oxide glass systems, these glasses are also candidates for non-linear optical applications and electro-optical devices [1–5].

There are four crystalline phases observed in tellurite glasses named as α-TeO_2, β-TeO_2, γ-TeO_2 and δ-TeO_2 [1–21].

Most of the tellurite glasses demonstrate α-TeO_2 structure such as TeO_2–K_2O, TeO_2–PbF_2 or TeO_2–BaF_2 glasses when subjected to heat-treatment [3–6]. α-TeO_2 phase also known as paratellurite, is formed by the constitution of the [TeO_4] units with a tetragonal structure only by sharing the corners hence the structure is three-dimensional. On the other hand, the β-TeO_2 phase is formed by sharing both the corners and edges hence the network is only two-dimensional [3,19].

The γ-TeO_2 phase has an orthorhombic crystal structure and also is formed in some of the tellurite glasses in the initial steps of the crystallization process. It is a metastable phase which transforms into the stable α-TeO_2 phase upon annealing at higher temperatures [1,5,7,16–18].

The γ-TeO_2 formation has been reported in some tellurite glasses such as TeO_2–WO_3 or TeO_2–PbO, TeO_2–Nb_2O_5–Bi_2O_3 [7,8,20].

The δ-TeO_2 phase was first observed by Blanchandin et al. [7]. It has a cubic structure and is an intermediate phase between the α-TeO_2 crystalline phase and glassy state. It was observed that the metastable δ-TeO_2 phase irreversibly transforms into the

* Corresponding author.
E-mail address: demettatar@yahoo.com (D. Tatar).

0272-8842/$36.00
doi:10.1016/j.ceramint.2011.10.023

stable α-TeO_2 phase in the TeO_2–WO_3 or TeO_2–PbF_2 glasses [5,6,21].

The composition of the tellurite glasses and the network structure is very important primarily because of the strong dependence of the coordination geometry of the Te atoms [1,3]. The addition of alkaline oxides in the TeO_2 structure changes the coordination of Te from a TeO_4 trigonal bipyramid group to a TeO_3 trigonal pyramid [1,3,16,22,23]. Tellurite glasses demonstrate a wide range of different properties mainly due to the type and the amount of the modifier in the glass composition [1–18,21–39].

For this reason, it is very important to study the glass forming systems of tellurium oxide with different metal oxides, fluorides or chlorides. Tellurite glasses with higher thermal stability values can be used as potential candidates as active media in solid-state lasers or fiber amplifiers [1,3,7,14–16,25–29].

This paper reports the investigations about the microstructural and thermal properties of the TeO_2–CdF_2–WO_3 glass systems which is a potential candidate in photonics [38].

2. Experimental procedure

2.1. Glass synthesis

Four different compositions with $0.85TeO_2$–$0.10CdF_2$–$0.05WO_3$, $0.80TeO_2$–$0.10CdF_2$–$0.10WO_3$, $0.75TeO_2$–$0.10CdF_2$–$0.15WO_3$ and $0.75TeO_2$–$0.15CdF_2$–$0.10WO_3$ in molar ratio were prepared by using high purity TeO_2 (99.99% purity, Aldrich), CdF_2 (99.90% purity, Aldrich) and WO_3 (99.90% purity, Aldrich) powders. Powder batches of 7 g were weighed in a Precisa™ XB220A sensitive balance and ground in an agate mortar for 5 min in order to obtain a homogenized structure. A platinum crucible with a closed lid was used for the melting processes in an electrically heated furnace at 900 °C for about 15–90 min. The molten sample was removed from the furnace at 900 °C and was cast by dipping the platinum crucible in icy-water bath for quenching.

2.2. Thermal behavior and crystallization

Differential thermal analysis (DTA) scans of as-cast $0.85TeO_2$–$0.10CdF_2$–$0.05WO_3$, $0.80TeO_2$–$0.10CdF_2$–$0.10WO_3$, $0.75TeO_2$–$0.10CdF_2$–$0.15WO_3$ and $0.75TeO_2$–$0.15CdF_2$–$0.10WO_3$ samples in molar ratio were carried out in TA™ Q600 DTA/TGA/DSC. The DTA scans were recorded using 3–15 mg as-cast specimens which were powdered and scanned with a heating rate of 20 °C/min between 20 and 800 °C in a platinum crucible by using same amount of alumina powder as the reference material. TA Instruments Universal Analysis Program™ was used to determine the glass transition temperature, T_g, selected as the inflection point of the step change of the calorimetric signal, the onset crystallization, T_c, and the crystallization peak temperatures, T_p, measured at the peak of crystallization. The heat-treated samples were prepared by heating the as-cast samples to the temperatures which are above the crystallization peak temperatures obtained from the DTA analyses and were quenched immediately by immersing the platinum crucible into icy-water bath.

2.3. Microstructural characterization

Scanning electron microscopy (SEM) investigations were carried out both in a JEOL™ Model JSM 5410 operated at 15 kV and linked with Noran™ 2100 Freedom energy dispersive spectrometer (EDS) attachment and in a JEOL™ Model JSM-T330 operated at 25 kV and linked with a Zmax 30 Boron-up light element EDS detector. All the samples were coated with palladium–gold for the SEM and SEM/EDS observations. To identify crystallizing phases in the glass matrix structures in the as-cast conditions and after annealing, X-ray diffraction (XRD) technique was performed on both as-cast glasses and heat-treated glass-ceramics using a Bruker™ D8 Advanced Series powder diffractometer. All traces were recorded using Cu Kα radiation and the diffractometer setting in the 2θ range from 20° to 80° by changing the 2θ with a step size of 0.02°. All samples were ground to fine powders for XRD investigations and Bruker™ Eva Software was used to label peaks and distinguish the crystalline phases existing in the sample. The International Centre for Diffraction Data® (ICDD) data files were used to identify the crystallized phases by comparing intensities and the peak positions in XRD scans.

3. Results and discussion

3.1. DTA investigations

Differential thermal analyses (DTA) were conducted on the as-cast $0.85TeO_2$–$0.10CdF_2$–$0.05WO_3$, $0.80TeO_2$–$0.10CdF_2$–$0.10WO_3$, $0.75TeO_2$–$0.10CdF_2$–$0.15WO_3$ and $0.75TeO_2$–$0.15CdF_2$–$0.10WO_3$ samples to understand the effects of WO_3 and the CdF_2 on the thermal behavior of the samples. Fig. 1 shows the DTA thermograms of these as-cast samples scanned between the temperatures of 200 °C and 800 °C with a heating rate of 20 °C/min. Table 1 lists glass transition, T_g, peak crystallization, T_p, melting temperatures, T_m, and the thermal stability values of the as-cast $0.85TeO_2$–$0.10CdF_2$–$0.05WO_3$, $0.80TeO_2$–$0.10CdF_2$–$0.10WO_3$, $0.75TeO_2$–$0.10CdF_2$–$0.15WO_3$ and $0.75TeO_2$–$0.15CdF_2$–$0.10WO_3$ samples obtained from their respective DTA thermograms in Fig. 1.

The DTA thermograms of the $0.85TeO_2$–$0.10CdF_2$–$0.05WO_3$ and $0.80TeO_2$–$0.10CdF_2$–$0.10WO_3$ and $0.75TeO_2$–$0.10CdF_2$–$0.15WO_3$ samples are similar and have two exotherms pertaining to crystallization and/or transformation of a crystalline phase or phases and two endotherms corresponding to melting.

For the $0.85TeO_2$–$0.10CdF_2$–$0.05WO_3$, $0.80TeO_2$–$0.10CdF_2$–$0.10WO_3$, $0.75TeO_2$–$0.10CdF_2$–$0.15WO_3$ samples which have the same CdF_2 content (10 mol% CdF_2) the glass transition and the melting temperatures increases with the increasing WO_3 content. Similar behavior was also be observed for the binary TeO_2–WO_3 glasses [7].

The $0.75TeO_2$–$0.15CdF_2$–$0.10WO_3$ sample differs from the other samples since it glass transition temperature was not clearly identified from its DTA thermogram. A small

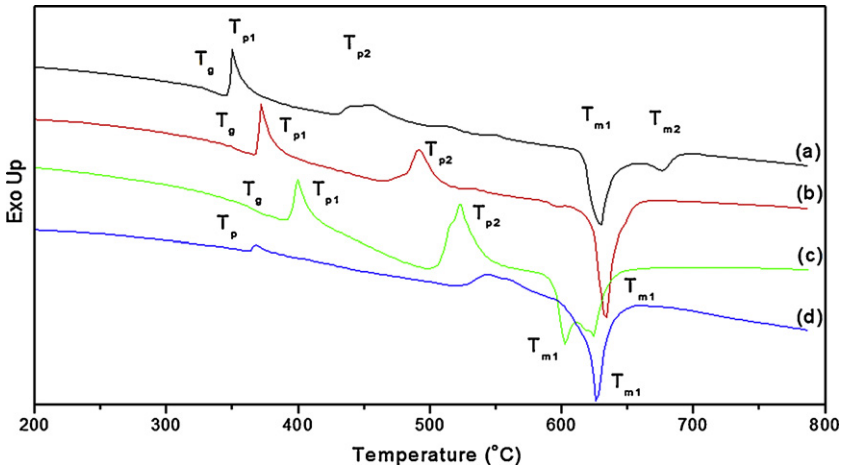

Fig. 1. DTA curves of the as-cast (a) $0.85TeO_2$–$0.10CdF_2$–$0.05WO_3$, (b) $0.80TeO_2$–$0.10CdF_2$–$0.10WO_3$, (c) $0.75TeO_2$–$0.10CdF_2$–$0.15WO_3$ and (d) $0.75TeO_2$–$0.15CdF_2$–$0.10WO_3$ samples scanned at a rate of 20 °C/min.

exothermic peak at around 368 °C and a convoluted exotherm occurring in the range of 530–570 °C for this sample might correspond to formations and/or transformations of some crystalline phases.

Difference between the first crystallization peak temperature (T_{p1}) and the glass transition temperature (T_g), ($\Delta T = T_c - T_g$) is a measure for the thermal stability of the glass against crystallization [9]. Thermal stability of the $0.85TeO_2$–$0.10CdF_2$–$0.05WO_3$, $0.80TeO_2$–$0.10CdF_2$–$0.10WO_3$, $0.75TeO_2$–$0.10CdF_2$–$0.15WO_3$ and $0.75TeO_2$–$0.15CdF_2$–$0.10WO_3$ as-cast samples are obtained by the DTA thermograms scanned at the heating rate of 20 °C/min and are listed in Table 1. It can be seen that the most thermally stable composition is the $0.75TeO_2$–$0.10CdF_2$–$0.15WO_3$ with a ΔT value of 34 °C, inferring that the addition of the WO_3 into the $(1-x)TeO_2$–$0.10CdF_2$–xWO_3 glasses (where $x = 0.05$, 0.10 and 0.15 in molar ratio), increases the thermal stability of the glass structure. Blanchandin et al. [7] reported that the thermal stability of TeO_2–WO_3 glasses regularly increases with the WO_3 content when the glasses are heated with a heating rate of 10 °C/min. which in between the ΔT value of 50 and 80 °C [7]. Comparing the ΔT values of the studied ternary TeO_2–CdF_2–WO_3 with the binary TeO_2–WO_3 glasses, it can be stated that the addition of the CdF_2 content into the binary TeO_2–WO_3 system decreases the thermal stability of the forming glasses.

3.2. X-ray diffractometry investigations

X-ray diffractometry (XRD) investigations were carried out on the basis of DTA thermograms in order to determine the crystallizing phases in both the as-cast samples and those heat-treated above peak crystallization temperatures. For all the compositions, XRD patterns were taken in the as-cast condition and after annealing at 420 °C and 560 °C which are chosen as temperatures just above the peak crystallization temperature.

Fig. 2(a)–(c) is the XRD patterns of the $0.85TeO_2$–$0.10CdF_2$–$0.05WO_3$ sample in the as-cast and annealed conditions. As can be seen from Fig. 2(a), the $0.85TeO_2$–$0.10CdF_2$–$0.05WO_3$ sample in the as-cast condition contains the δ-TeO_2 phase (Bravais lattice: f.c.c., $a = 0.569$ nm) (Blanchandin et al. [7]; ICDD, 42-1365) in its glassy matrix. As stated by Blanchandin et al. [7], it is not possible to obtain the δ-TeO_2 phase from pure TeO_2 samples, but it can be synthesized from different solid solutions such as $Pb_{1-x}Te_xF_{2-2x}O_{2x}$ or $Cd_{1-x}Te_xF_{2-2x}O_{2x}$. The lattice parameter observed in the as-cast $0.85TeO_2$–$0.10CdF_2$–$0.05WO_3$sample of the present study is smaller than the reported values (Blanchandin et al. [7]; ICDD, 42-1365). Even though the formation of the δ-TeO_2 phase was not observed in any of the studied binary TeO_2–CdF_2 glass compositions, the present study shows that within the ternary TeO_2–CdF_2–WO_3 system, it is possible to observe the δ-TeO_2 phase [13,14]. As seen in Fig. 2(b) when the $0.85T5eO_2$–$0.10CdF_2$–$0.05WO_3$ sample is annealed at 420 °C, γ-TeO_2 phase (orthorhombic structure, $a = 0.4898$ nm, $b = 0.8576$ nm, $c = 0.4351$ nm) forms along with the δ-TeO_2 phase (ICDD, 42-1365; ICDD, 52-1005). Using least squares approximation on XRD peaks of Fig. 2(b), the average value for the lattice parameter of the δ-TeO_2 phase was calculated as $a = 0.552$ nm which is less than that of the same phase existing in the as-cast condition.

Table 1
Glass transition (T_g), crystallization peak (T_p), melting (T_m) temperatures and the thermal stability of the $0.85TeO_2$–$0.10CdF_2$–$0.05WO_3$, $0.80TeO_2$–$0.10CdF_2$–$0.10WO_3$, $0.75TeO_2$–$0.10CdF_2$–$0.15WO_3$ and $0.75TeO_2$–$0.15CdF_2$–$0.10WO_3$ samples.

Sample	T_g (°C)	T_{p1} (°C)	T_{p2} (°C)	T_{m1} (°C)	T_{m2} (°C)	ΔT ($T_{p1} - T_g$)
$0.85TeO_2$–$0.10CdF_2$–$0.05WO_3$	329	350	454	629	676	21
$0.80TeO_2$–$0.10CdF_2$–$0.10WO_3$	348	372	491	633	–	24
$0.75TeO_2$–$0.10CdF_2$–$0.15WO_3$	365	399	523	602	624	34
$0.75TeO_2$–$0.15CdF_2$–$0.10WO_3$	–	–	544	626	–	–

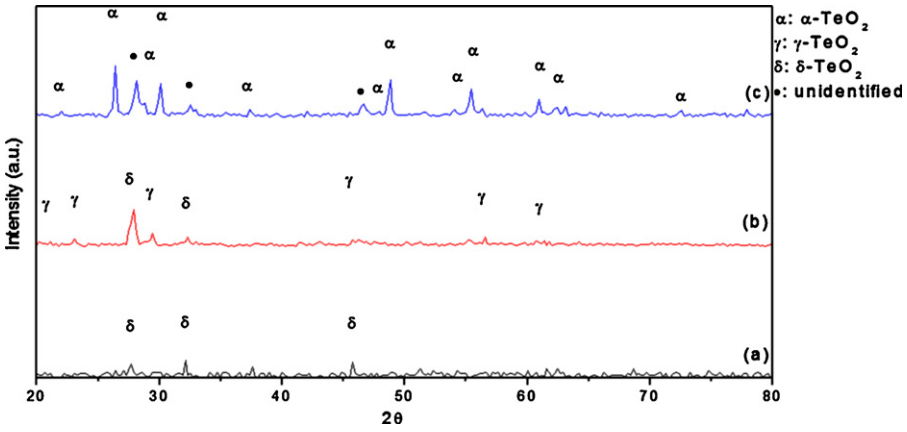

Fig. 2. XRD scans taken from the $0.85TeO_2$–$0.10CdF_2$–$0.05WO_3$ sample in the form of (a) as-cast, (b) annealed at 420 °C for 30 min and (c) annealed at 560 °C for 30 min.

Further heat-treatment of the glass at 560 °C results in the transformation of the metastable δ-TeO_2 and γ-TeO_2 phases into the stable α-TeO_2 phase (tetragonal crystal structure, $a = 0.481$ nm and $c = 0.761$ nm) which can be seen in Fig. 2(c) [16]. In addition, a new phase which is labeled as unidentified in Fig. 2(c) with relatively high intensities is formed at 560 °C. The determination of the crystal structure and the lattice parameters of this new phase is part of an ongoing study and will be published elsewhere.

Fig. 3(a)–(c) is the respective XRD patterns of the $0.80TeO_2$–$0.10CdF_2$–$0.10WO_3$ glass in the as-cast condition and after annealing at 420 and 560 °C for 30 min. It is evident from Fig. 3(a) that the $0.80TeO_2$–$0.10CdF_2$–$0.10WO_3$ sample has an amorphous structure in the as-cast condition. However, when the glass is annealed at 420 °C for 30 min, the metastable δ-TeO_2 and γ-TeO_2 phases are formed (Fig. 3(b)). The lattice parameter of the δ-TeO_2 phase was calculated as $a = 0.560$ nm which is smaller than the card value (ICDD, 42-1365). Similar to the $0.85TeO_2$–$0.10CdF_2$–$0.05WO_3$ sample, when the $0.80TeO_2$–$0.10CdF_2$–$0.10WO_3$ glass is annealed at 560 °C for 30 min, the metastable δ-TeO_2 and γ-TeO_2 phases transform to the stable α-TeO_2 phase (Fig. 3(c)). The unidentified phase is also present in the structure of the $0.80TeO_2$–$0.10CdF_2$–$0.10WO_3$ sample annealed at 560 °C for 30 min (Fig. 3(c)).

Fig. 4(a)–(c) is a series of XRD patterns of the $0.75TeO_2$–$0.10CdF_2$–$0.15WO_3$ glass in the as-cast condition, and after annealing at 420 and 560 °C, respectively. As seen in Fig. 4(a), similar to the as-cast $0.80TeO_2$–$0.10CdF_2$–$0.10WO_3$ glass, the $0.75TeO_2$–$0.10CdF_2$–$0.15WO_3$ sample has an amorphous structure in the as-cast condition. When the glass is annealed at 420 °C for 30 min, the δ-TeO_2 phase and also very little amount of γ-TeO_2 crystals are formed in the microstructure. As expected, due to δ-TeO_2/γ-TeO_2 to α-TeO_2 transformations, only the stable α-TeO_2 phase, WO_3, and the new unidentified phase are observed in the microstructure of the same glass annealed at 560 °C for 30 min (Fig. 4(c)). Unlike the $0.85TeO_2$–$0.10CdF_2$–$0.05WO_3$ and $0.80TeO_2$–$0.10CdF_2$–$0.10WO_3$ glasses which have less than 10 mol% WO_3 contents, the formation of the WO_3 phase (orthorhombic crystal structure; $a = 0.738$ nm, $b = 0.751$ nm and $c = 0.385$ nm) takes place in the $0.75TeO_2$–$0.10CdF_2$–$0.15WO_3$ glass which contains 15 mol% WO_3. The presence of the orthorhombic WO_3 phase was also observed in the binary TeO_2–WO_3 glass system containing 15 mol% WO_3 [20].

Fig. 5(a)–(d) is the XRD patterns of the $0.75TeO_2$–$0.15CdF_2$–$0.10WO_3$ sample in the as-cast condition and after annealing at 420 °C for 30 min and at 560 °C for 30 and 120 min, respectively. As can be seen in Fig. 5(a), the

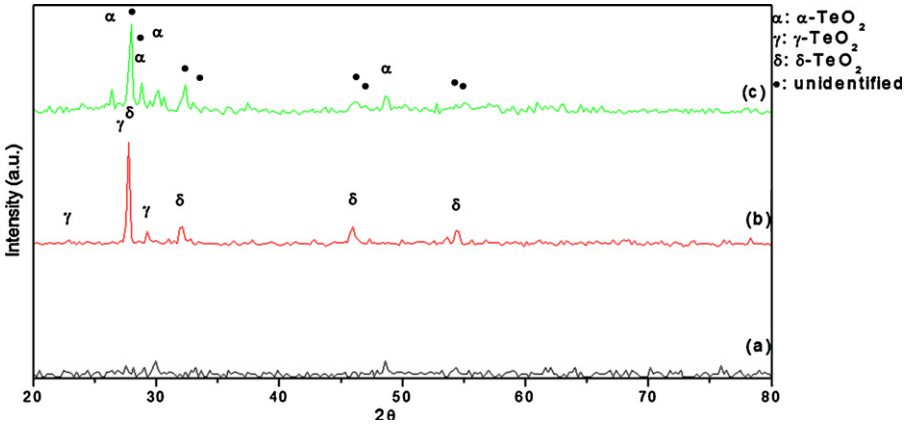

Fig. 3. XRD scans taken from the $0.80TeO_2$–$0.10CdF_2$–$0.10WO_3$ sample in the form of: (a) as-cast, (b) annealed at 420 °C and (c) annealed at 560 °C for 30 min.

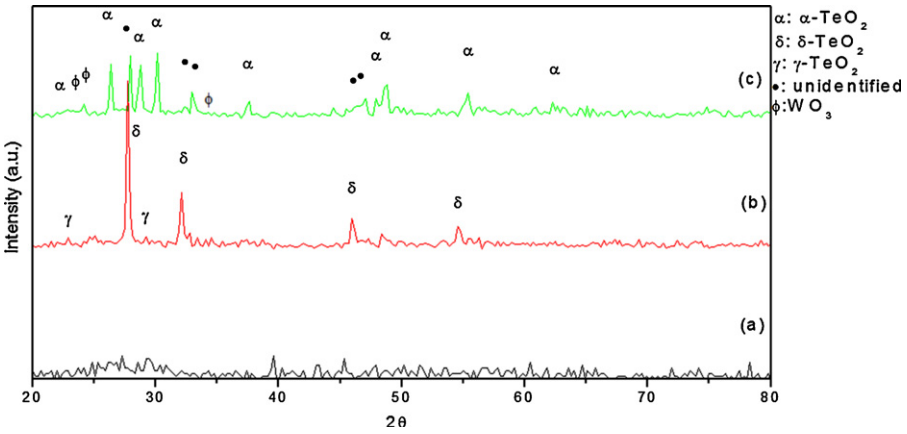

Fig. 4. XRD scans taken from the $0.75TeO_2$–$0.10CdF_2$–$0.15WO_3$ sample in the form of (a) as-cast, (b) annealed at 420 °C for 30 min and (c) annealed at 560 °C for 30 min.

$0.75TeO_2$–$0.15CdF_2$–$0.10WO_3$ sample does not have an amorphous structure in the as-cast condition and contains the metastable δ-TeO_2 phase. The δ-TeO_2 phase exists as the only crystalline formation in the structure in the as-cast condition and when the sample is annealed at 420 °C and at 560 °C for 30 min (Fig. 5). However, when the annealing time is increased to 120 min at 560 °C, the δ-TeO_2 phase completely transforms to the stable α-TeO_2 phase (Fig. 5(d)). In addition to the α-TeO_2 crystalline phase a new unidentified phase and also $CdTe_2O_5$ crystalline phase (monoclinic crystal structure; $a = 0.681$ nm, $b = 0.384$ nm, $c = 0.985$ nm and $\beta = 115.2°$) emerge in the microstructure (ICDD, 49-1755). The increase of the CdF_2 content results in the formation of the $CdTe_2O_5$ phase in the annealed structure of the $0.75TeO_2$–$0.15CdF_2$–$0.10WO_3$ sample containing 15 mol% CdF_2 (Fig. 5(d)) while the increase of the WO_3 content results in the formation of the WO_3phase in the annealed structure of the $0.75TeO_2$–$0.10CdF_2$–$0.15WO_3$ sample containing 15 mol% WO_3 (Fig. 4(c)).

Table 2 summarizes all the crystalline phases identified in the as-cast and annealed $0.85TeO_2$–$0.10CdF_2$–$0.05WO_3$, $0.80TeO_2$–$0.10CdF_2$–$0.10WO_3$, $0.75TeO_2$–$0.10CdF_2$–$0.15WO_3$ and $0.75TeO_2$–$0.15CdF_2$–$0.10WO_3$ samples. As stated previously, on the basis of XRD scans of all compositions (Figs. 2–5), for the $0.85TeO_2$–$0.10CdF_2$–$0.05WO_3$ and $0.80TeO_2$–$0.10CdF_2$–$0.10WO_3$ samples, the formation of the metastable γ-TeO_2 phase, and then the transformation of this phase into stable α-TeO_2 phase and the unidentified phase are listed in Table 2. The first exotherms in the DTA thermograms of all compositions (Fig. 1) correspond to the formation of the metastable γ-TeO_2 and/or δ-TeO_2 phases, and the second ones are due to the transformation of these metastable phases into the stable α-TeO_2 and the unidentified phase. Similar behavior is also observed for the TeO_2–CdF_2, TeO_2–WO_3 and some other TeO_2-based glass systems [3,4,31,39]. The WO_3 and $CdTe_2O_5$ phases are observed only in the microstructures of the $0.75TeO_2$–$0.10CdF_2$–$0.15WO_3$ and $0.75TeO_2$–$0.15CdF_2$–$0.10WO_3$ samples, so it can be concluded that the formation of the WO_3 and $CdTe_2O_5$ phases occur when the respective WO_3 and CdF_2 amounts are 15 mol% in the ternary TeO_2–CdF_2–WO_3 glasses.

3.3. SEM and SEM/EDS investigations

In order to reveal the morphology of the crystallizing phases, SEM and SEM/EDS investigations were conducted

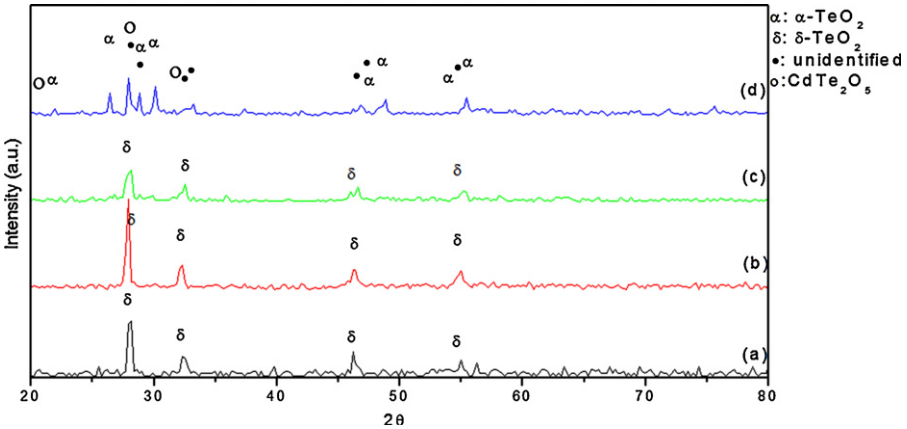

Fig. 5. XRD scans taken from the $0.75TeO_2$–$0.15CdF_2$–$0.10WO_3$ sample in the form of (a) as-cast condition, (b) annealed at 420 °C for 30 min and (c) annealed at 560 °C for 30 min and (d) annealed at 560 °C for 2 h.

Table 2
Crystalline phases determined in the as-cast and annealed $0.85TeO_2$–$0.10CdF_2$–$0.05WO_3$, $0.80TeO_2$–$0.10CdF_2$–$0.10WO_3$, $0.75TeO_2$–$0.10CdF_2$–$0.15WO_3$ and $0.75TeO_2$–$0.15CdF_2$–$0.10WO_3$ samples.

Composition	As-cast	420 °C 30 min	560 °C 30 min	560 °C 2 h
$0.85TeO_2$–$0.10CdF_2$–$0.05WO_3$	δ-TeO_2	δ-TeO_2 γ-TeO_2	α-TeO_2 Unidentified	–
$0.80TeO_2$–$0.10CdF_2$–$0.10WO_3$	Amorphous	δ-TeO_2 γ-TeO_2	α-TeO_2 Unidentified	–
$0.75TeO_2$–$0.10CdF_2$–$0.15WO_3$	Amorphous	δ-TeO_2 γ-TeO_2	α-TeO_2 Unidentified WO_3	–
$0.75TeO_2$–$0.15CdF_2$–$0.10WO_3$	δ-TeO_2	δ-TeO_2	δ-TeO_2	α-TeO_2 Unidentified $CdTe_2O_5$

ICDD, 42-1365; ICDD, 52-1005; ICDD, 52-0796; ICDD, 49-1755; ICDD, 20-1324.

on the $0.85TeO_2$–$0.10CdF_2$–$0.05WO_3$, $0.80TeO_2$–$0.10CdF_2$–$0.10WO_3$, $0.75TeO_2$–$0.10CdF_2$–$0.15WO_3$ and $0.75TeO_2$–$0.15CdF_2$–$0.10WO_3$ samples. For all samples, surface SEM micrographs were taken in the secondary electron imaging (SEI) mode. According to the XRD investigations (Fig. 2(b)), when the $0.85TeO_2$–$0.10CdF_2$–$0.05WO_3$ sample is annealed at 420 °C for 30 min, δ-TeO_2 and γ-TeO_2 phases crystallize in the microstructure.

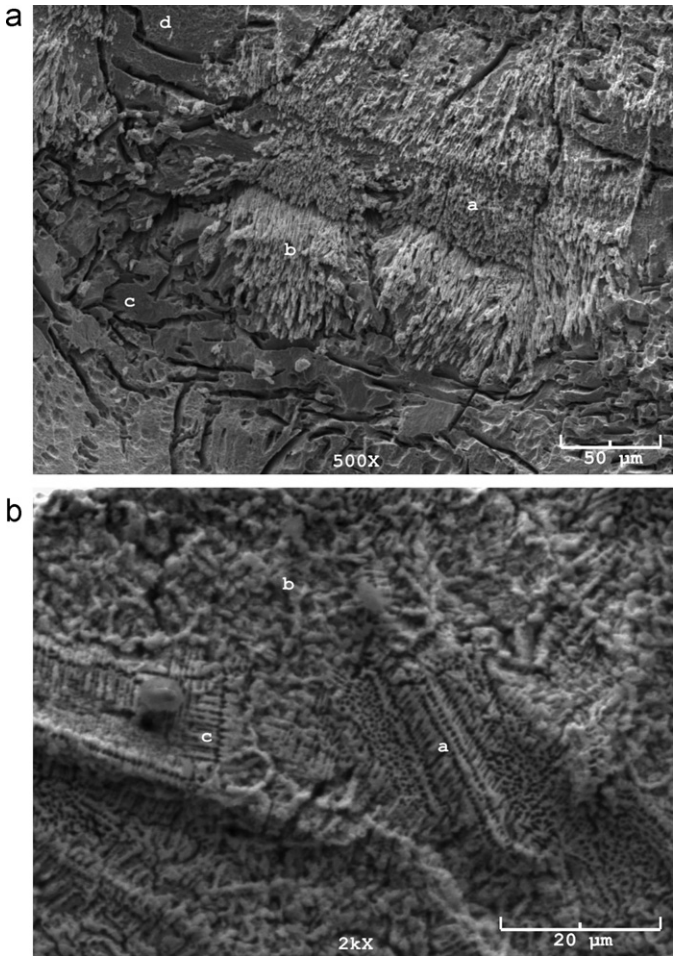

Fig. 6. Typical SEM micrographs taken from the crystalline regions of the $0.85TeO_2$–$0.10CdF_2$–$0.05WO_3$ sample: (a) annealed at 420 °C for 30 min and (b) annealed at 560 °C for 30 min.

Fig. 6(a) is a representative SEM/SEI micrograph of the surface of the $0.85TeO_2$–$0.10CdF_2$–$0.05WO_3$ sample heat-treated at 420 °C followed by quenching. EDS spectra taken from different locations on these crystals have shown that the regions labeled with 'c' and 'd' contain 32.55 ± 0.8 at.% Te, 4.22 ± 0.3 at.% W, 2.92 ± 0.3 at.% Cd, 61.34 ± 0.2 at.% O and the regions labeled with 'a' and 'b' contain 38.59 ± 0.5 at.% Te, 6.09 ± 0.4 at.% W, 2.92 ± 0.3 at.% Cd, 51.18 ± 0.7 at.% O, indicating that the needle-like formations labeled with a and b are TeO_2-rich crystals surrounded by a glassy matrix labeled with 'c' and 'd'.

Fig. 6(b) is a SEM/SEI micrograph of the $0.85TeO_2$–$0.10CdF_2$–$0.05WO_3$ sample annealed at 560 °C for 30 min. According to the XRD investigations given in Fig. 2(c), the α-TeO_2 and a new unidentified crystalline phases are present in the microstructure of the $0.85TeO_2$–$0.10CdF_2$–$0.05WO_3$ sample annealed at 560 °C for 30 min. EDS spectra taken from different regions in Fig. 6(b) show that the regions labeled with 'a' and 'c' contain 34.89 ± 0.3 at.% Te, 3.61 ± 0.5 at.% W, 1.56 ± 0.3 at.% Cd, 59.94 ± 0.2 at.% O and the region labeled with 'b' contains 27.57 ± 0.5 at.% Te, 3.17 ± 0.4 at.% W, 3.17 ± 0.3 at.% Cd, 67.38 ± 0.7 at.% O the indicating that the crystals formations labeled with 'a' and 'c' are TeO_2-rich crystals. Due to the fact that the different morphology types of paratellurite formations are known in other studies, it can be suggested that the disordered crystals labeled with 'b' given in Fig. 6(b) belong to the paratellurite phase [16,17]. Hence the small blocks of ordered crystals labeled with 'a' and 'c' in Fig. 6(b) might belong to the unidentified phase.

Fig. 7(a) and (b) are typical SEM/SEI micrographs of the $0.80TeO_2$–$0.10CdF_2$–$0.10WO_3$ sample annealed at 420 and 560 °C, respectively. According to the XRD investigations given in Fig. 3(b), when the $0.80TeO_2$–$0.10CdF_2$–$0.10WO_3$ glass is annealed at 420 °C for 30 min, δ-TeO_2 and γ-TeO_2 phases crystallize in the microstructure (Fig. 7(a)). EDS spectra taken from different locations on these crystals show that the region labeled with 'a' contains 26.90 ± 0.5 at.% Te, 4.55 ± 0.4 at.% W, 2.26 ± 0.5 at.% Cd, 66.29 ± 0.5 at.% O, the region labeled

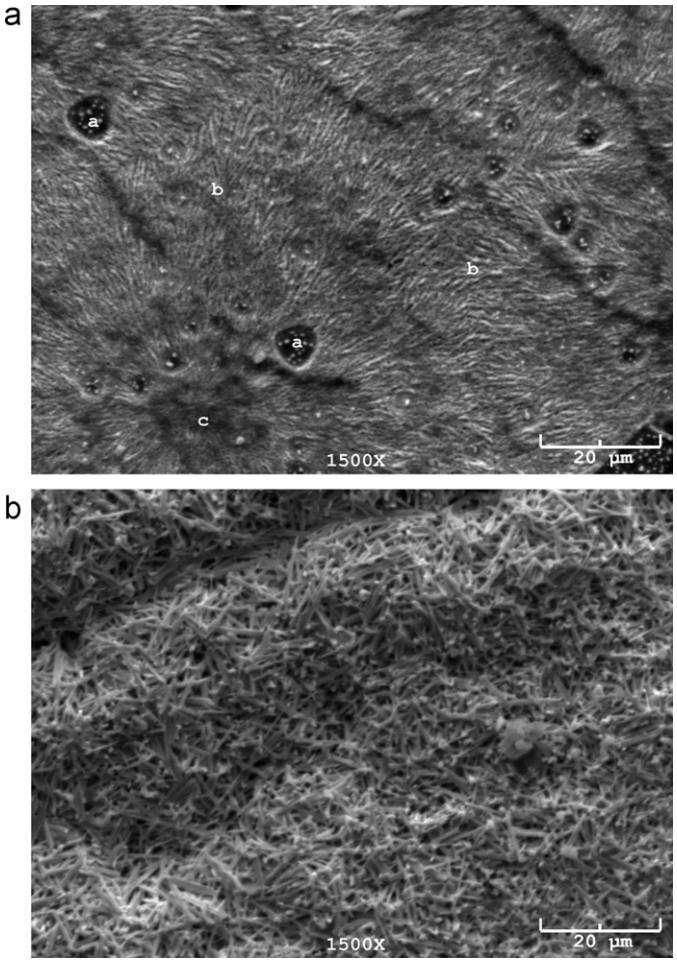

Fig. 7. Typical SEM micrographs taken from the crystalline regions of the $0.80TeO_2$–$0.10CdF_2$–$0.10WO_3$ sample: (a) annealed at 420 °C for 30 min and (b) annealed at 560 °C for 30 min.

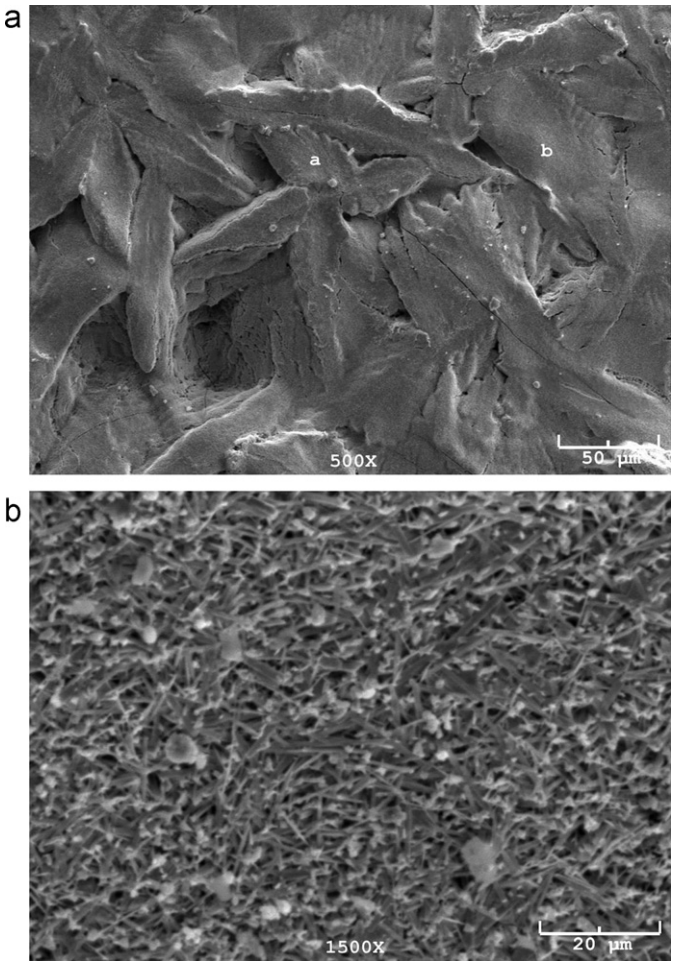

Fig. 8. Typical SEM micrographs taken from the crystalline regions of the $0.75TeO_2$–$0.10CdF_2$–$0.15WO_3$ sample: (a) surface region annealed at 420 °C for 30 min and (b) surface region annealed at 560 °C for 30 min.

with 'b' contains 23.86 ± 0.5 at.% Te, 5.00 ± 0.4 at.% W, 3.47 ± 0.6 at.% Cd, 67.78 ± 0.7 at.% O and the region labeled with 'c' contains 21.18 ± 0.4 at.% Te, 5.32 ± 0.5 at.% W, 3.72 ± 0.5 at.% Cd, 69.78 ± 0.7 at.% O. This indicates that all the crystal formations labeled with 'a', 'b' and 'c' are TeO_2-rich crystals and therefore it is not possible to determine the identity of these crystalline phases via EDS results. According to the XRD scans of Fig. 3(c), when the $0.80TeO_2$–$0.10CdF_2$–$0.10WO_3$ sample is annealed at 560 °C for 30 min, it consists of α-TeO_2 and the unidentified phase in its structure. It can be seen from Fig. 7(b) that the $0.80TeO_2$–$0.10CdF_2$–$0.10WO_3$ sample heat-treated at 560 °C has a completely different microstructural morphology than that of the same sample annealed at 420 °C. Fig. 7(b) demonstrates that disoriented and needle-like crystals form when the sample is annealed at 560 °C.

Fig. 8(a) and (b) is typical SEM micrographs taken from the $0.75TeO_2$–$0.10CdF_2$–$0.15WO_3$ sample annealed at 420 and 560 °C, respectively. According to the XRD investigations (Fig. 4(b)), when the $0.75TeO_2$–$0.10CdF_2$–$0.15WO_3$ glass is annealed at 420 °C for 30 min, it comprises the δ-TeO_2 and γ-TeO_2 crystalline phases in its microstructure. Fig. 8(a) is a representative SEM/SEI micrograph of the $0.75TeO_2$–$0.10CdF_2$–$0.15WO_3$ sample heat treated at 420 °C for 30 min. EDS spectra taken from different locations in these crystals show that the regions labeled with 'a' contains 17.59 ± 0.4 at.% Te, 4.70 ± 0.3 at.% W, 3.53 ± 0.3 at.% Cd, 74.18 ± 0.2 at.% O and the regions labeled with 'b' contains 17.44 ± 0.4 at.% Te, 4.18 ± 0.4 at.% W, 4.32 ± 0.6 at.% Cd, 74.06 ± 0.4 at.% O. Fig. 8(b) is a SEM micrograph of the surface region of the $0.75TeO_2$–$0.10CdF_2$–$0.15WO_3$ sample heat treated at 560 °C for 30 min. According to the XRD investigations (Fig. 4(c)) when the $0.75TeO_2$–$0.10CdF_2$–$0.15WO_3$ glass is annealed at 560 °C for 30 min, it demonstrates α-TeO_2, WO_3 and the unidentified phase in its structure. It can clearly be seen that the crystalline morphologies that are formed in Fig. 8(a) and (b) are different. Crystals formed when the $0.75TeO_2$–$0.10CdF_2$–$0.15WO_3$ glass was annealed at 420 °C for 30 min are relatively larger than the ones formed when the glass was annealed at 560 °C for 30 min. The crystal formations shown in Fig. 8(a) are leaf-like. On the other hand the crystal formations shown in Fig. 8(b) are disoriented and needle-like and show a similar microstructure to the ones given in Fig. 7(b).

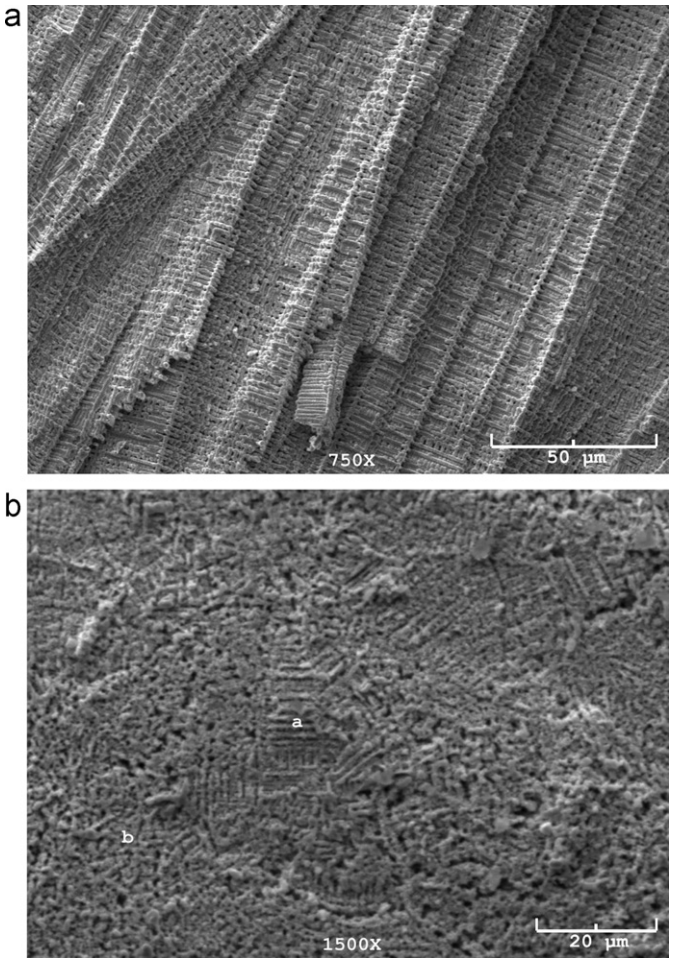

Fig. 9. Typical SEM micrographs taken from the crystalline regions of the $0.75TeO_2$–$0.15CdF_2$–$0.10WO_3$ sample: (a) in the as-cast condition, respectively, (b) annealed at 560 °C for 2 h.

Fig. 9(a) and (b) demonstrates typical SEM micrographs taken from the $0.75TeO_2$–$0.15CdF_2$–$0.10WO_3$ sample. As it can be seen in Fig. 9(a), regular array of crystals which resemble long lines of vertebra-like structures are dominant in the $0.75TeO_2$–$0.15CdF_2$–$0.10WO_3$ sample in the as-cast condition. These formations belong solely to the δ-TeO_2 phase, as revealed by the XRD scan of Fig. 5(a)–(c) revealing that the δ-TeO_2 phase is the only crystalline phase in this sample in the as-cast condition and also after annealing at 420 °C and 560 °C for 30 min. The morphology of the δ-TeO_2 phase can be observed solely in the $0.75TeO_2$–$0.15CdF_2$–$0.10WO_3$ sample in the as-cast condition and heat-treated at 420 and 560 °C for 30 min. Fig. 9(a) is given as a representative SEM image for the same microstructures of the samples in the as-cast condition and heat-treated at 420 and 560 °C for 30 min. Fig. 9(b) is a representative SEM micrograph taken from the surface of the $0.75TeO_2$–$0.15CdF_2$–$0.10WO_3$ sample annealed at 560 °C for 2 h. In Fig. 9(b), it can be seen that the regular array of crystals are no longer existing in the structure of the sample annealed at 560 °C for 2 h.

According to the XRD investigations given in Fig. 5(d), when the $0.75TeO_2$–$0.15CdF_2$–$0.10WO_3$ sample is annealed at 560 °C for 2 h, α-TeO_2, $CdTe_2O_5$ and the unidentified phases form in the microstructure. EDS spectra taken from different locations on these crystals show that, the region labeled with 'a' contains 25.869 ± 0.5 at.% Te, 3.527 ± 0.5 at.% W, 4.806 ± 0.5 at.% Cd, 65.700 ± 0.5 at.% O and the region labeled with 'b' contains 22.518 ± 0.5 at.% Te, 3.935 ± 0.5 at.% W, 4.490 ± 0.5 at.% Cd, 69.056 ± 0.5 at.% O. This indicates that the crystal formations labeled with 'a' belong to the TeO_2-rich crystals and therefore it is not possible to determine the identity of these crystalline phases via EDS results.

4. Conclusions

On the basis of the results obtained from the DTA/DSC, XRD and SEM/EDS analyses, the following conclusions can be drawn:

1. Among the compositions studied in the ternary TeO_2–CdF_2–WO_3 system, only the $0.80TeO_2$–$0.10CdF_2$–$0.10WO_3$ and the $0.75TeO_2$–$0.10CdF_2$–$0.15WO_3$ samples consist of amorphous glassy structure under conventional quenching conditions.
2. The DTA thermograms of the $0.85TeO_2$–$0.10CdF_2$–$0.05WO_3$, $0.80TeO_2$–$0.10CdF_2$–$0.10WO_3$ and $0.75TeO_2$–$0.10CdF_2$–$0.15WO_3$ samples are similar and have two exotherms pertaining to crystallization or transformation of a phase. The two endotherms in these samples correspond to melting processes. DTA investigations show that increasing the WO_3 content causes an increase in the glass transition, T_g, and the crystallization temperatures, T_c. The addition of the WO_3 content increases the thermal stability of the ternary TeO_2–CdF_2–WO_3 system. Hence, the most thermally stable composition of the present investigation is the $0.75TeO_2$–$0.10CdF_2$–$0.15WO_3$ sample with a ΔT value of 34 °C. On the contrary, the addition of CdF_2 content decreases the thermal stability.
3. XRD investigations conducted on the samples in the as-cast and annealed conditions demonstrate that the $0.85TeO_2$–$0.10CdF_2$–$0.05WO_3$, $0.80TeO_2$–$0.10CdF_2$–$0.10WO_3$ and $0.75TeO_2$–$0.10CdF_2$–$0.15WO_3$ samples have the metastable δ-TeO_2 and γ-TeO_2 phases in their structure when these samples are annealed at 420 °C for 30 min. On the other hand, the $0.75TeO_2$–$0.15CdF_2$–$0.10WO_3$ sample only has the metastable δ-TeO_2 in its structure. The second exothermic peaks for the $0.85TeO_2$–$0.10CdF_2$–$0.05WO_3$, $0.80TeO_2$–$0.10CdF_2$–$0.10WO_3$ and $0.75TeO_2$–$0.10CdF_2$–$0.15WO_3$ samples are convoluted peaks and refer to the transformation of the δ-TeO_2 and/or γ-TeO_2 metastable phases into the stable α-TeO_2 and an unidentified phase. In addition, for the $0.75TeO_2$–$0.10CdF_2$–$0.15WO_3$ and $0.75TeO_2$–$0.15CdF_2$–$0.10WO_3$ samples, the second exothermic peaks also include the formations of the WO_3 and $CdTe_2O_5$ phases. The transformation of the metastable δ-TeO_2 phase into the stable α-TeO_2 phase takes place when the sufficient time of 2 h is completed.
4. SEM/EDS investigations reveal that the morphology of the δ-TeO_2 phase is observed solely in the $0.75TeO_2$–$0.15CdF_2$–$0.10WO_3$ sample in the as-cast condition and heat-treated at 420 and 560 °C for 30 min.

References

[1] A.H. El-Mallawany, Tellurite Glasses Handbook, second ed., CRS Press, London, 2002.

[2] M. Matterelli, A. Chiappini, M. Montagna, A. Martucci, A. Ribaudo, M. Guglielmi, M. Ferrari, A. Chiasera, Optical spectroscopy of TeO_2–GeO_2 glasses activated with Er^{3+} and Tm^{3+} glasses, J. Non-Cryst. Solids 351 (2005) 1759–1763.

[3] M. O'Donnell, Tellurite and Fluorotellurite Glasses for Active and Passive Fibreoptic Waveguides. Ph.D. Thesis, The University of Nottingham, UK, 2004.

[4] B. Öz, M.L. Öveçoğlu, İ. Kabalcı, G. Özen, Microstructural characterization and crystallization kinetics of $(1-x)TeO_2$–xK_2O (x = 0.05, 0.10, 0.15, 0.20 mol) glasses, J. Eur. Ceram. Soc. 27 (2007) 3239–3251.

[5] M.L. Öveçoğlu, İ. Kabalcı, G. Özen, B. Öz, Microstructural characterization of $(1-x)TeO_2$–$xPbF_2$ (x = 0.10 and 0.25 mol) glasses, J. Eur. Ceram. Soc. 27 (2007) 1801–1804.

[6] A.N. Begum, V. Rajendran, Structure and elastic properties of TeO_2–BaF_2 glasses, J. Phys. Chem. Solids 67 (2006) 1697–1702.

[7] S. Blanchandin, P. Marchet, P. Thomas, J.C. Champarnaud-Mesjard, B. Frit, New investigations within the TeO_2–WO_3 system: phase equilibrium diagram and glass crystallization, J. Mater. Sci. 34 (1999) 4285–4292.

[8] M.A.P. Silva, Y. Messaddeq, S.J.L. Ribeiro, M. Poulain, F. Villain, V. Briois, Structural studies on TeO_2–PbO glasses, J. Phys. Chem. Solids 62 (2001) 1055.

[9] E.R. Shaaban, M.T. Dessouky, A.M. Abousehly, Glass forming tendency in ternary $Ge_xAs_{20}Te_{80-x}$ glasses examined using differential scanning calorimetry, J. Phys. Condens. Matter 19 (2007) 096212.

[10] M.A.P. Silva, Y. Messaddeq, V. Briois, M. Poulain, F. Villian, S.J.L. Ribeiro, Synthesis and structural investigations on TeO_2–CdF_2–PbF_2 glasses and transparent glass–ceramics, J. Phys. Chem. Solids 63 (2002) 605–609.

[11] G. Wang, S. Dai, J. Zhang, L. Wen, J. Yang, Z. Jiang, Thermal, optical properties and structural investigation of TeO_2–$PbCl_2$ glassy system, J. Phys. Chem. Solids (2005) 1–5.

[12] A. Nukui, T. Taniguchi, M. Miyata, In situ high-temperature X-ray observation of structural changes of tellurite glasses with p-block oxides; ZnO–TeO_2 glasses, J. Non-Cryst. Solids 293 (2001) 255.

[13] D. Tatar, M.L. Öveçoğlu, G. Özen, Microstructural characterization and crystallization of $(1-x)TeO_2$–$xCdF_2$ (x = 0.10, 0.15, 0.25 mol) glasses, J. Eur. Ceram. Soc. 16 (2008) 3097–3106.

[14] D. Tatar, M.L. Öveçoğlu, G. Özen, F.B. Erim, Glass transition and crystallization of $0.8TeO_2 + 0.2CdF_2$ glass, J. Eur. Ceram. Soc. 29 (2009) 329–335.

[15] D. Tatar, G. Özen, F.B. Erim, M.L. Öveçoğlu, Raman characterizations and structural properties of binary TeO_2–WO_3 TeO_2–CdF_2 and ternary TeO_2–CdF_2–WO_3 glasses, J. Raman Spectrosc. 41 (7) (2009) 797–807.

[16] D. Tatar, M.L. Öveçoğlu, G. Özen, S.A. Speakman, Microstructural characterization and crystallization kinetics of $(1-x)TeO_2$–$0.10CdF_2$–$xPbF_2$ (x = 0.05 0.010, and 0.15 mol) glasses, J. Mater. Res. 24 (10) (2009) 3087–3094.

[17] M. Udovic, P. Thomas, A. Mirgorodsky, O. Durand, M. Soulis, O. Masson, T. Merle-Mejean, J.C. Champarnaud-Mesjard, Thermal characteristics, Raman spectra and structural properties of new tellurite glasses within the Bi_2O_3–TiO_2–TeO_2 system, J. Solid State Chem. 179 (2006) 3252–3259.

[18] A.P. Mirgorodsky, T. Merle-Mejean, J.C. Camparnaud, P. Thomas, B. Frit, Dynamics of structure of TeO_2 polymorphs: model treatment of paratellurite and tellurite: Raman scattering evidence for new γ-TeO_2 and δ-TeO_2 phases, J. Phys. Chem. 61 (2000) 501–509.

[19] S. Blanchandin, P. Thomas, P. Marchet, J.C. Champarnaud-Mesjard, B. Frit, New heavy metal oxide glasses: investigations within the TeO_2–Nb_2O_5–Bi_2O_3 system, J. Alloys Compd. 347 (2002) 206–212.

[20] M.L. Öveçoğlu, G. Özen, S. Cenk, Microstructural characterization and crystallization behavior of $(1-x)TeO_2$–xWO_3 (x = 0.15 0.25, 0.3 mol) glasses, J. Eur. Ceram. Soc. 26-7 (2006) 1149–1158.

[21] J.C. Sabadel, P. Armand, F. Terki, J. Pelous, D. Cachau-Herreillat, E. Philippot, Brillouin and low frequency Raman studies of TeO_2–BaO–TiO_2 glasses, J. Phys. Chem. Solids 61 (2000) 745–1750.

[22] V. Rajendran, N. Palanivelu, B.K. Chaudhuri, K. Goswami, Characterization of semiconducting V_2O_5–Bi_2O_3–TeO_2 glasses through ultrasonic measurements, J. Non-Cryst. Solids 320 (2003) 195–209.

[23] M.D. O'Donnell, K. Richardson, R. Stolen, C. Rivero, T. Cardinal, M. Couzi, D. Furniss, A.B. Seddon, Raman gain of selected tellurite glasses for IR fiber lasers calculated from spontaneous scattering spectra, Opt. Mater. 30 (2008) 946–951.

[24] C. Rivero, R. Stegeman, K. Richardson, G. Stegeman, G. Turri, G.M. Bass, P. Thomas, M. Udovic, T. Cardinal, E. Fargin, M. Couzi, H. Jain, A. Miller, Influence of modifier oxides on the structural and optical properties of binary TeO_2 glasses, J. Appl. Phys. 101 (2007) 023526.

[25] A. Kanoun, N. Jaba, A. Brenier, Time-resolved up-converted luminescence in Er^{3+}-doped TeO_2–ZnO glass, Opt. Mater. 26 (2004) 79–83.

[26] C.R. Eyzaguirre, E. Rodriguez, E. Fernandez Chillcce, S.P.A. Osorio, C.L. Cesar, C.L. Barbosa, Use of CsCl to enhance the glass stability range of tellurite glasses for Er^{3+}-doped optical fiber drawing, J. Am. Ceram. Soc. 90 (6) (2007) 1822–1826.

[27] S. Xu, G. Wang, J. Zhang, S. Dai, L. Hu, Z. Jiang, Composition dependent upconversion of Er^{3+}-doped PbF_2–TeO_2 glasses, J. Non-Cryst. Solids 336 (2004) 230–233.

[28] M. Jayasimhadri, L.R. Moorthy, K. Kojima, K. Yamamoto, N. Wada, N. Wada, Er^{3+}-doped tellurofluorophosphate glasses for lasers and optical amplifiers, J. Phys. Condens. Matter 17 (2005) 7705–7715.

[29] Z. Shang, G. Ren, Q. Yang, C. Xu, Y. Liu, Y. Zhang, Q. Wu, Spectroscopic properties of Er^{3+}-doped and Er^{3+}/Yb^{3+}-codoped PbF_2–MO_x (M = Te, Ge, B) oxyfluoride glasses, J. Alloys Compd. 467 (2009) 351–356.

[30] H. Lin, S. Tanabe, L. Lin, D.L. Yang, K. Liu, W.H. Wong, J.Y. Yu, E.Y.B. Pun, Infrequent blue and green emission transitions from Eu^{3+} in heavy metal tellurite glasses with low phonon energy, Phys. Lett. A 358 (2006) 474–477.

[31] C. Jiang, P. Deng, J. Zhang, F. Gan, Emission properties of ytterbium-doped GeO_2–TeO_2 glasses, Phys. Lett. A 324 (2004) 91–94.

[32] P. Charton, P. Armand, X-ray absorption and Raman characterizations of TeO_2–Ga_2O_3 glasses, J. Non-Cryst. Solids 333 (2004) 307–315.

[33] A. Mekki, G.D. Khattak, L.E. Wenger, Structural and magnetic properties of MoO_3–TeO_2 glasses, J. Non-Cryst. Solids 351 (2005) 2493–2500.

[34] P. Charton, P. Thomas, P. Armand, Raman and crystallization behaviors of TeO_2–Sb_2O_4 glasses, J. Non-Cryst. Solids 321 (2003) 81–88.

[35] B.V.R. Chowdari, P.P. Kumari, Raman spectroscopic study of ternary silver tellurite glasses, Mater. Res. Bull. 2 (34) (1999) 327–342.

[36] M. Soulis, A.P. Mirgorodsky, T. Merle-Méjean, O. Masson, P. Thomas, M. Udovic, The role of modifier's cation valence in structural properties of TeO_2-based glasses, J. Non-Cryst. Solids 354 (2008) 143–149.

[37] S.M. Lima, W.F. Falco, E.S. Bannwart, L.H.C. Andrade, R.C. Oliveira, J.C.S. Moraes, K. Yukimitu, E.B. Araujo, E.A. Falcao, A. Steimacher, N.C.G. Astrath, A.C. Bento, A.N. Medina, M.L. Baesso, Thermo-optical characterization of tellurite glasses by thermal lens thermal relaxation calorimetry and interferometric methods, J. Non-Cryst. Solids 352 (2006) 3603–3607.

[38] G. Bilir, G. Özen, D. Tatar, Judd–Ofelt analysis and near infrared emission properties of the Er^{3+} ions in tellurite glasses containing WO_3 and CdO, Opt. Commun. 284 (3) (2011) 863–868.

[39] R. Akagi, K. Handa, N. Ohtori, A.C. Hannon, M. Tatsumisago, N. Umesaki, High-temperature structure of K_2O–TeO_2 glasses, J. Non-Cryst. Solids 256–257 (1999) 111–118.